Chapter 6
Ice Detection on Plate Structures Using Modal Curvature and Piezoelectric Sensor Networks

Lorenzo Stagi, Nicola Roveri, Salvatore Ameduri, Antonio Concilio, and Jean-François Deü

Abstract Ice accretion on engineering structures such as aircraft and wind turbines can severely compromise safety and efficiency, highlighting the need for reliable detection and localization strategies. In this work, a modal-based methodology is proposed to identify ice on plate-like structures exploiting deviations in curvature mode shapes, reconstructed using a network of piezoelectric transducers, between a reference ice-free state and the iced configuration. Both numerical and experimental investigations were carried out on the same aluminum plate instrumented with 42 piezoelectric patches, enabling direct comparison between simulation and measurements.

Numerical simulations were first performed to assess the method's sensitivity to different ice geometries and thicknesses. The analysis considered both curvature mode shapes and their spatial derivatives, showing that the use of second derivatives significantly improves localization accuracy, particularly in the presence of irregular or distributed ice patterns. The same plate was then tested experimentally, with paraffin patches employed as ice surrogates. Operational Modal Analysis techniques were used to extract mode shapes from frequency response functions, and the proposed localization algorithm was applied.

Results consistently confirmed the numerical findings, with the second derivative of curvature providing the most explicit and robust localization of the iced regions. The study highlights the potential of modal curvature analysis, combined with a dense piezoelectric array, as an effective and lightweight strategy for spatially resolved ice detection. Moreover, the same transducer network could be subsequently exploited for active ice removal, paving the way toward fully integrated sensing–actuation systems for autonomous de-icing.

Keywords Piezoelectric · Ice detection · Curvature mode shapes · Curvature derivatives · Structural health monitoring

Introduction

Ice formation poses a significant challenge in both wind energy and aviation sectors, where it compromises safety, reduces operational efficiency, and accelerates structural degradation. On wind turbine blades, even moderate ice buildup alters the aerodynamic profile, leading to power losses of up to 50% annually, while simultaneously increasing fatigue loads and inducing structural imbalance, thereby shortening service life [1]. In aviation, icing affects boundary-layer behavior, reducing lift, increasing drag and stall speed, and may ultimately lead to hazardous loss-of-control incidents [2].

Current ice detection methods are mostly indirect [3], relying on performance degradation metrics combined with environmental data such as temperature and humidity. However, these approaches lack responsiveness and do not provide precise

Lorenzo Stagi · Nicola Roveri
Department of Mechanical and Aerospace Engineering, Sapienza University of Rome, Rome, Italy
e-mail: lorenzo.stagi@uniroma1.it; nicola.roveri@uniroma1.it

Salvatore Ameduri · Antonio Concilio
Italian Aerospace Research Centre (CIRA), Capua, Italy
e-mail: S.Ameduri@cira.it; A.Concilio@cira.it

Jean-François Deü
Structural Mechanics Laboratory, Conservatoire National des Arts et Métiers, Paris, France
e-mail: jean-francois.deu@lecnam.net

Kristin B. Zimmerman, PhD (eds.), *Topics in Modal Analysis & Parameter Identification in Structural Dynamics, 2026, Vol. 8*,
Conference Proceedings of the Society for Experimental Mechanics Series, https://doi.org/10.1007/978-8-743-81447-4_6

information about the ice's location or quantity. A reliable, real-time, and spatially resolved detection system would not only improve flight safety but also enhance the efficiency of de-icing systems by enabling targeted intervention.

Piezoelectric sensor networks represent a promising solution [4]: when bonded or embedded into a structure, they can cover large surface areas with minimal added weight and aerodynamic penalty, while also providing quantitative information on the extent and morphology of ice deposits. Among the various sensing strategies, electromechanical impedance (EMI) methods have gained considerable attention; these methods are based on monitoring variations in the electrical impedance of the piezoelectric transducers, which reflect changes in the mechanical properties of the host structure. For example, Zhang et al. [5] demonstrated the feasibility of using EMI indicators combined with neural network classifiers for reliable ice detection on cables. Building on this work, Maio et al. [6] showed that applying principal component analysis enhances sensitivity in composite plates. More recently, Wiedemann et al. [7] proposed an integrated approach for helicopter rotor blades, where impedance variations are used for ice detection and low-frequency excitations actively remove ice accumulations.

Although electromechanical-impedance features remain an active research direction, the most widely adopted approach for icing detection is based on ultrasonic guided-wave interrogation [8]. In this method, piezoelectric transducers bonded to the structure generate and receive propagating Lamb waves. Well established in Structural Health Monitoring (SHM) and non-destructive testing of thin plates, this technique exploits the high sensitivity of Lamb-wave attenuation, velocity, and mode conversion to structural inhomogeneities; by tracking these parameters, information about defect size and location can be inferred [9, 10, 11]. The same principle extends to icing: an accreted ice layer perturbs the Lamb-wave field through scattering, additional damping, and phase-velocity shifts. Several researchers have demonstrated this effect. Zhang et al. [12] developed a delay-based algorithm that identifies ice by measuring the additional travel time of a wave packet relative to a baseline; their approach was validated experimentally on a plate with two piezoelectric elements and an intervening ice patch. Similarly, Pohl [13] designed a local sensor that detects ice through concurrent variations in amplitude and velocity. For spatial mapping, Zhao et al. [14] introduced a probability-based reconstruction method capable of accurately identifying the geometry of ice deposits.

Ice can also be detected by exploiting changes in modal parameters, such as natural frequencies and mode shapes, caused by ice accretion. Gantasala et al. [15] showed that such changes could be used to detect and quantify ice. Later, the same author introduced a neural network-based method that, using natural frequencies as input, could estimate both the quantity and location of ice with a weighted average percentage error of 17.53%. In a related effort, Tsiapoki et al. [16] applied a similar frequency-based neural network model to a full-scale wind turbine blade, further validating this approach.

In the present study, a modal strategy is adopted to perform ice localization by analyzing changes in the curvature mode shapes of the structure. The use of modal curvature is a well-established approach in SHM [17, 18], where it has been widely employed for damage detection and localization due to its high sensitivity to local stiffness variations. By extending this concept to icing scenarios, the present work investigates whether curvature-based indicators can also provide robust and spatially resolved information on ice accretion. Deviations between measured and reference curvature mode shapes are exploited to detect and localize ice accretion, with the most affected regions exhibiting the largest discrepancies. Furthermore, a specific focus of this work is to investigate whether operating on the derivatives of the curvature mode shapes can enhance detection performance.

The proposed algorithm was first validated numerically and subsequently tested experimentally. A simplified setup was implemented using a $420 \times 360\ mm$ aluminum plate instrumented with 42 piezoelectric transducers. An additional feature of this setup is its potential integration with an active de-icing strategy, whereby the same network could be used not only for detection but also for ice removal once accretion is identified. In this context, Song et al. [19] developed a de-icing approach on a plate-like structure similar to the one investigated in this work, combining piezoelectric actuation with a genetic algorithm, enabling the system to maximize the stresses required to break the ice precisely where it is present while leaving the rest of the structure unaffected. This result highlights the strong potential of piezoelectric networks to serve as both sensing and actuation platforms, paving the way toward fully integrated solutions for autonomous ice management.

Curvature Derivatives and Local Effects

The study of higher-order derivatives of curvature mode shapes has already been carried out for beam-like structures in [20]. Here, the key steps of that formulation are recalled. Moreover, for exposition clarity, the one dimensional formulation is considered; the two dimensional generalization follows by replacing $\phi'' = \kappa_{i,j}$ and $\phi^{iv} = \Delta^4\phi$. Consider an Euler–Bernoulli beam with spatially varying elastic and inertial properties. The modal equation of motion is

$$(EI(x)\,\phi''(x))'' + \rho(x)A(x)\,\omega^2\phi(x) = 0, \tag{1}$$

where $\phi(x)$ is the mode shape, $EI(x)$ the flexural rigidity, and $\rho(x)A(x)$ the mass per unit length. Defining the modal curvature as $\kappa(x) = \phi''(x)$, the equation can be rewritten as

$$EI(x)\,\kappa''(x) + 2(EI)'(x)\,\kappa'(x) + (EI)''(x)\,\kappa(x) + \rho(x)A(x)\,\omega^2\phi(x) = 0. \tag{2}$$

Dividing by $\phi(x)$ yields the local relation

$$\frac{\kappa''(x)}{\phi(x)} = -\frac{\rho(x)A(x)}{EI(x)}\,\omega^2 - 2\,\frac{(EI)'(x)}{EI(x)}\,\frac{\kappa'(x)}{\phi(x)} - \frac{(EI)''(x)}{EI(x)}\,\frac{\kappa(x)}{\phi(x)}. \tag{3}$$

This expression shows how higher-order derivatives of curvature reflect local variations in structural properties. In homogeneous systems, with constant EI and ρA, the derivative terms vanish and the ratio κ''/ϕ reduces to the constant value $-(\rho A/EI)\,\omega^2$, with no spatial variation. When stiffness varies, however, the terms involving $(EI)'/EI$ and $(EI)''/EI$ introduce localized peaks in κ'/ϕ and κ/ϕ, making them sensitive to cracks, stiff patches, or mechanical inhomogeneities. Conversely, mass variations mainly affect the baseline of κ''/ϕ through the term $-(\rho A/EI)\,\omega^2$, without necessarily producing localized discontinuities.

From this derivation, it follows that higher-order derivatives amplify local changes: while curvature κ already reflects stiffness through its proportionality to bending moment, κ' and κ'' emphasize gradients and discontinuities, offering a more discriminating diagnostic tool. The drawback is their sensitivity to noise, which makes regularization or filtering strategies necessary in experiments.

In the context of icing, a deposited patch increases local stiffness and produces mass addition, influencing all the terms κ'/ϕ and κ/ϕ and shifting the baseline of κ''/ϕ. This distinction allows deviations observed in experimental data to be directly associated with the structural modifications induced by ice accretion. Based on these considerations, the proposed methodology evaluates not only the reconstructed modal curvature from the piezoelectric network but also its first and second derivatives in order to investigate whether the enhanced sensitivity can improve the localization of iced regions.

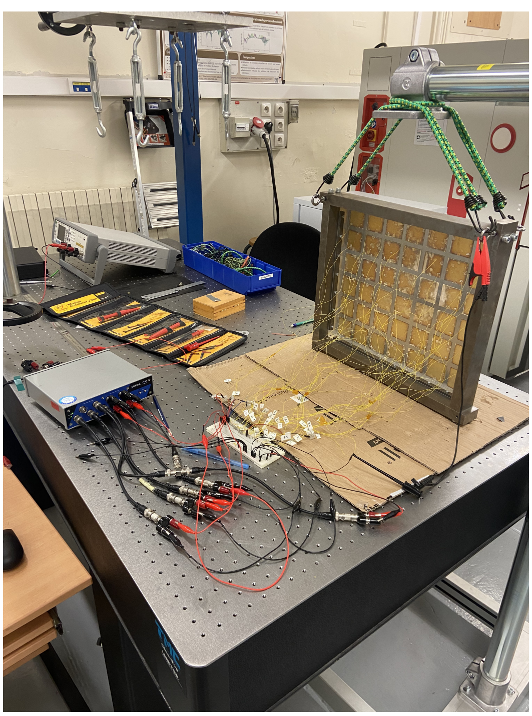

Fig. 1 Picture of the plate from which it is possible to notice the yellow patches (the piezoelectric transducer) and the steel frame

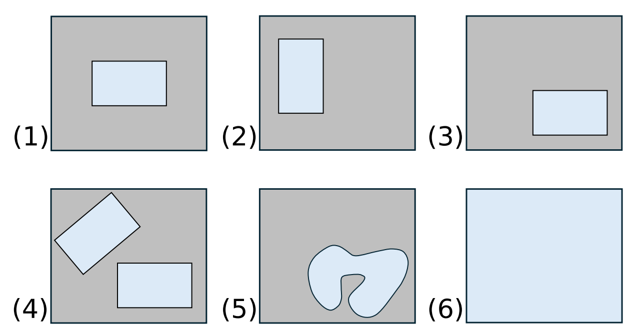

Fig. 2 Position of the patch of ice for the six analyzed configurations. In case 6 the patch covers all the plate

Table 1 Geometrical configurations and thickness for different analyzed configurations

Condition	Dimension [mm]	Thickness [mm]
1	200×120	2
2	200×120	2
3	200×120	2
4	2 patches of 200×120	2
5	*irregular shape*	2
6	420×360	5

Model description

The study focuses on a simply supported aluminum rectangular plate with dimensions $l_x = 420\ mm$, $l_y = 360\ mm$, and thickness $h_s = 3\ mm$. The plate is instrumented with 42 square piezoelectric transducers (side length $l_p = 50\ mm$, thickness $h_p = 0.5\ mm$), manufactured using PIC 153 piezoelectric material (PI Ceramic). Figure 1 shows the experimental setup. The plate is mounted on a steel frame through $0.5\ mm$ aluminum strips, which provide sufficient longitudinal stiffness to prevent transverse displacement while offering low flexural rigidity to approximate free rotational boundary conditions.

The model was validated against the analytical natural frequencies of the simply supported plate. According to classical plate theory, the natural frequencies are given by

$$f_{(m,n)} = h_s \left(\frac{m^2}{l_x^2} + \frac{n^2}{l_y^2} \right) \frac{\pi}{4} \sqrt{\frac{Y_s}{3\rho_s \left(1 - \nu_s^2\right)}}, \tag{4}$$

where $f_{(m,n)}$ is the natural frequency of the (m, n) mode, h_s is the plate thickness, l_x and l_y are the plate dimensions along the x and y directions, respectively, m and n are the half-wave numbers in the x and y directions, Y_s is the Young's modulus, ρ_s is the density, and ν_s is the Poisson's ratio.

The accuracy of the numerical model was assessed by comparing its natural frequencies with those obtained analytically and experimentally. As shown in Figure 3, the three sets of results are in close agreement, with discrepancies consistently below 8%, and typically around 4% for the experimental and numerical cases. These differences are mainly attributed to the bonded piezoelectric patches, which are not considered in the analytical formulation but are included in both the numerical model and the experimental setup, as well as to slight inconsistencies in reproducing the boundary conditions in the experimental configuration. A detailed description of the setup is provided in [21].

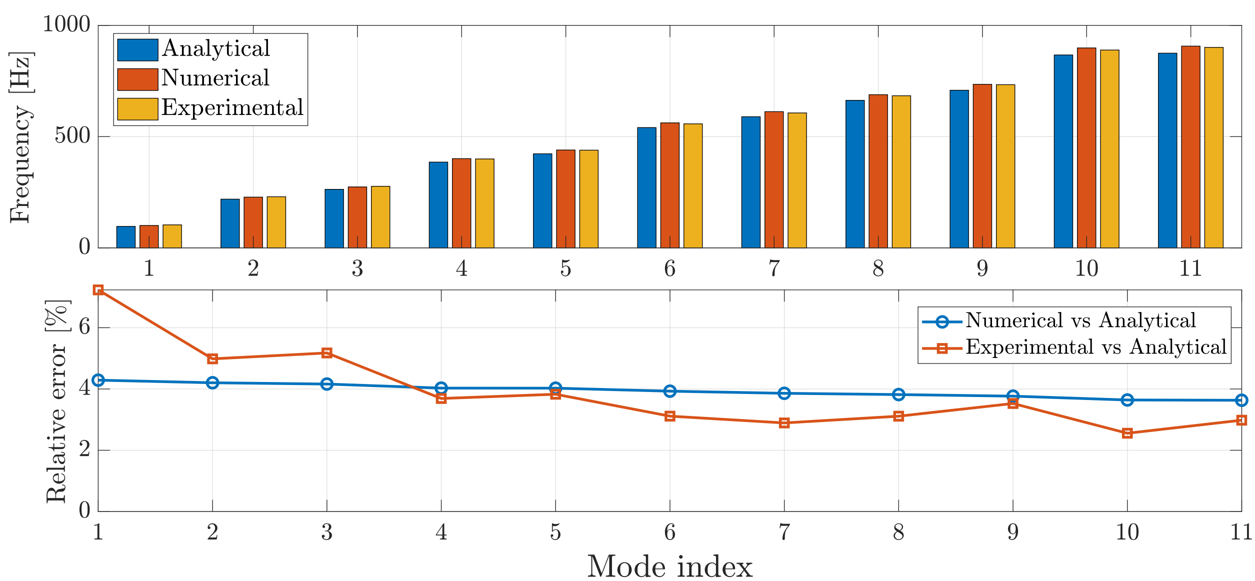

Fig. 3 Comparison of the first eleven natural frequencies from analytical, numerical, and experimental results, with discrepancies below 8% due to the presence of piezoelectric patches not included in the analytical model

Methodology

The proposed detection algorithm is based on the voltage response of the piezoelectric sensors, which is proportional to the average in-plane deformation of the plate. These measurements are used to reconstruct the curvature mode shapes. In this study, up to 11 vibration modes were considered within the 0–1000 Hz frequency range.

To minimize variability, the reconstructed curvature mode shapes were normalized by dividing each sensor's response by that of a reference sensor (Patch 11 in Figure 5), selected to ensure non-zero output across all modes. Subsequently, the

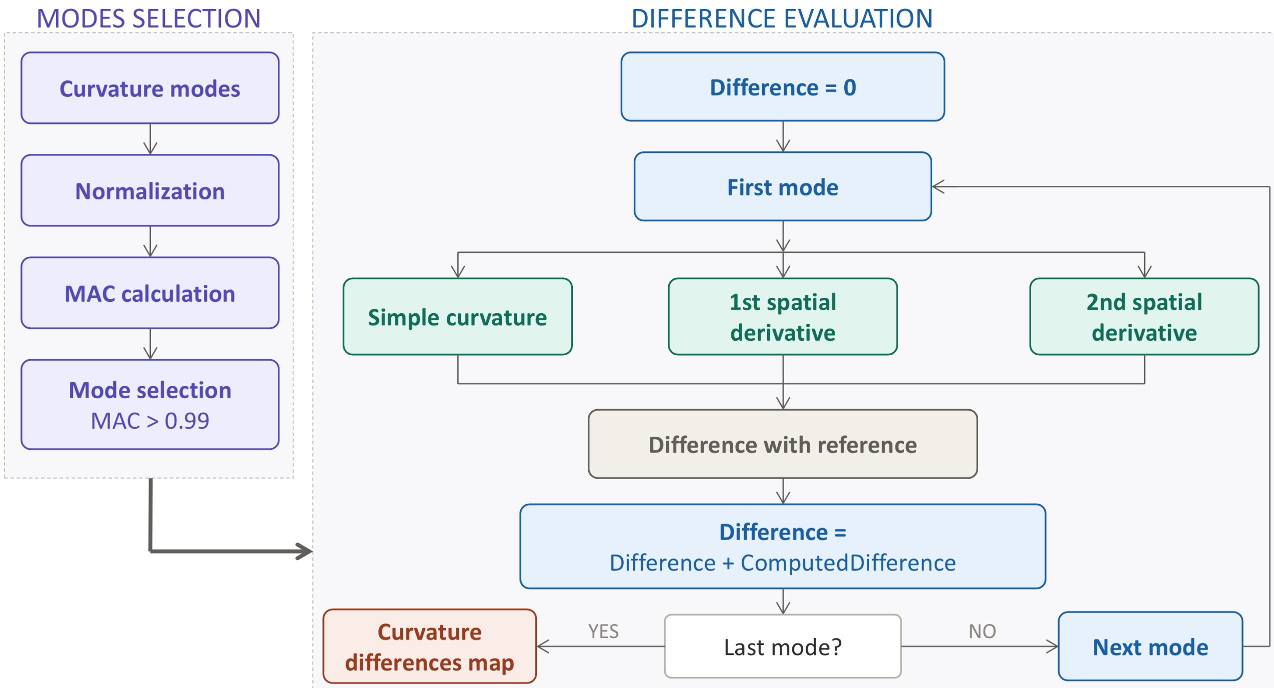

Fig. 4 Block scheme of the algorithm in the three cases when curvature differences are considered and when the first and second derivative of the curvature is employed

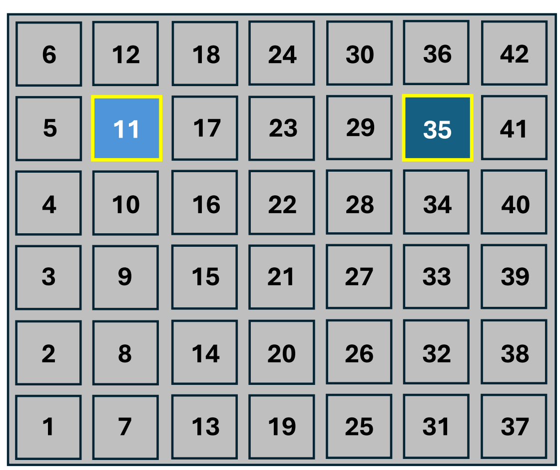

Fig. 5 Layout of the 42 piezoelectric transducers mounted on the plate. Transducer 11 was selected as the reference sensor for the normalization procedure, while transducer 35 was used as the actuator during the experimental tests

second spatial derivative of the curvature mode shapes was computed to assess whether higher-order derivatives improve ice localization performance.

For the iced configurations, the extracted modes were compared with those of the ice-free reference case using the Modal Assurance Criterion (MAC). Only modes with a MAC greater than 0.99 were retained for analysis, ensuring that the comparison focused on modes strongly consistent with the reference case. This filtering minimizes the impact of discrepancies and highlights modal shape variations specifically induced by ice accretion. Localization was carried out by summing, for each sensor, the deviations between the reference and current curvature mode shapes across the selected modes.

The methodology was tested on six different ice configurations, varying in size, thickness, and position (Figure 2, Table 1). Case 6 represents full-surface icing, whereas Cases 1–5 correspond to localized patches of different geometries. The overall algorithmic workflow is summarized in Figure 4.

To quantitatively assess the performance of the localization algorithm, an index was introduced that evaluates how well the most significant portion of the localization map overlaps with the true patch. Let $H(x, y)$ denote the localization map normalized in $[0, 1]$, and let Ω be the set of all pixels (or sensor positions). The pixels are first ranked in descending order according to the values of $H(x, y)$, and the subset $\Omega_k \subset \Omega$ containing the top $k\%$ of pixels is selected. The localization index is then defined as

$$T_k = \frac{|\Omega_k \cap P|}{|\Omega_k|}, \tag{5}$$

where P denotes the set of pixels belonging to the actual patch.

In this work, the value $k = 10\%$ was chosen, so that the index measures the fraction of the 10% most activated pixels of the map that are located inside the true patch. By construction, $T_k \in [0, 1]$: values close to 1 indicate that the most relevant part of the localization map is concentrated within the actual patch, thus reflecting a good localization, whereas values close to 0 correspond to cases in which the algorithm's strongest response lies outside the true patch. Compared to centroid-based measures, this formulation directly assesses the spatial consistency between the detected high-intensity region and the actual patch, while remaining insensitive to distortions or multiple maxima in the map.

It is worth noting that this index is meaningful for all test cases except for the last one (Case 6), where the ice patch completely covers the plate surface. In such a situation, T_k would trivially take the value 1 regardless of the localization map, and thus provides little information on the actual performance of the algorithm. For this specific case, a qualitative graphical evaluation was therefore preferred.

Numerical Analysis

The numerical investigation was conducted using COMSOL Multiphysics. The aluminum plate and the ice patches were modeled as perfectly bonded, forming a single composite domain. Modal analysis was performed to extract the mode shapes and corresponding voltages at each piezoelectric patch (Figure 6 illustrates representative results for the second and seventh modes).

When the curvature mode shapes were directly employed as input to the localization algorithm, the method was able to provide a satisfactory indication of the iced regions in all six test cases (Figure 7, first column). The identified areas generally overlapped with the actual patch locations, which are indicated in the figures, demonstrating the capability of curvature-based indicators to capture the main alterations induced by the ice. Nonetheless, the resolution of the results was not always optimal: in Case 4, the presence of two distinct patches modified the global response of the plate, leading to a more diffuse localization, while in Case 5, the irregular geometry of the ice layer produced a broader and less defined affected region.

The introduction of spatial derivatives enhanced the performance of the method. The first derivative of curvature (Figure 7, second column) yielded slightly sharper contours of the localized regions compared to curvature alone, but the improvement remained marginal, and in some cases the results were comparable.

By contrast, the second derivative of curvature (Figure 7, third column) produced a significant improvement in localization accuracy. The detected regions appeared more compact and better aligned with the actual patches. For Cases 1–3, where the ice coverage followed simple geometries, the iced areas were reconstructed with higher precision and reduced spatial spreading. In Case 5, the irregular patch was captured more reliably, with the algorithm reproducing its main shape and extension. In Case 6, characterized by uniform ice coverage, the method correctly highlighted the distributed nature of the modification across the entire plate. Table 2 provides the quality index accordingly to Equation 5 for the numerical case.

Experimental Analysis

For the experimental investigation, one of the 42 piezoelectric transducers mounted on the plate was used as an actuator (transducer 35 in Figure 5), while the voltages induced in the remaining 41 sensors were recorded. The transducer selected for excitation was chosen to ensure effective activation of all eleven target modes. The input signal consisted of a linear chirp ranging from 20 to 1000 Hz. The acquisition system provided the frequency response functions (FRFs) of each sensor

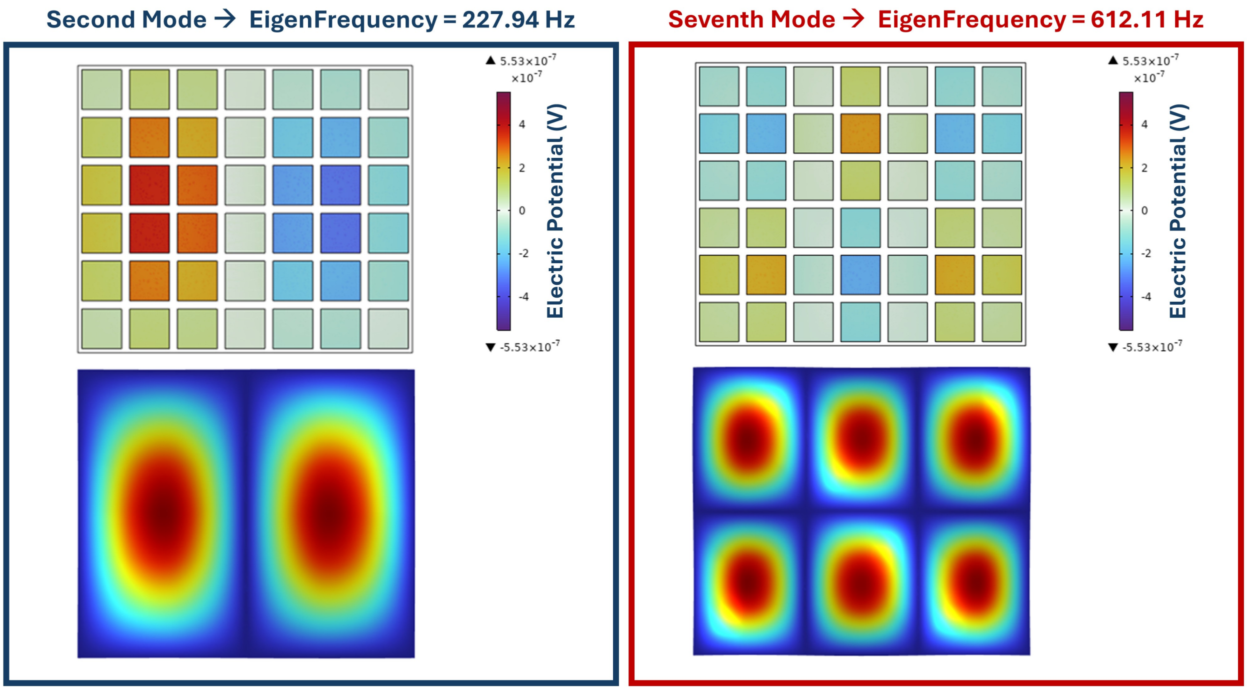

Fig. 6 Voltages measured from each piezoelectric patch for the numerical analysis. In the figure, the cases for the second and seventh modes are reported, in the figures above the voltages, and in the plots below the mode shapes

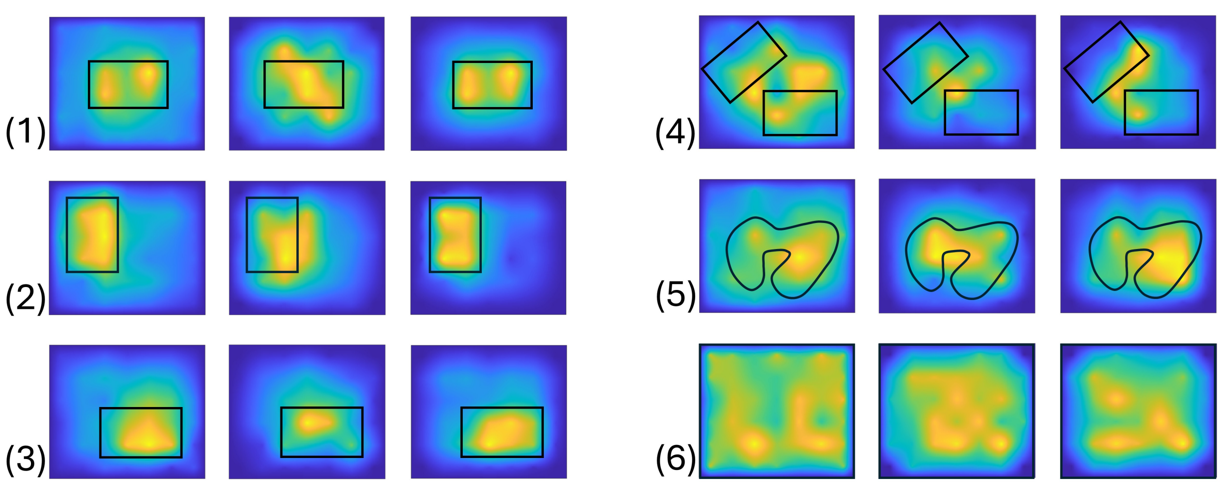

Fig. 7 Ice localization maps for the six analyzed configurations. Each row corresponds to a different ice scenario (Cases 1–6, see Table 1), while the three columns represent the localization algorithm applied to: (left) curvature mode shapes, (center) first spatial derivative of curvature mode shapes, and (right) second spatial derivative of curvature mode shapes. For each case, the actual patch location is indicated in the figures. Warmer colors indicate stronger deviations from the ice-free reference, highlighting the regions most affected by ice accretion

directly. To reduce measurement noise, five repeated acquisitions were performed for each configuration, and the corresponding FRFs were averaged prior to further processing.

The exported FRFs were analyzed using operational modal analysis techniques to estimate the natural frequencies and mode shapes. The Least-Squares Complex Exponential algorithm [22] was employed to extract modal parameters directly from the frequency responses. Since the measured voltages are proportional to structural curvature, the resulting identified mode shapes correspond to curvature mode shapes. Subsequently, point-by-point differences between the reference and

Table 2 Quantitative evaluation of the localization performance for different ice conditions. The reported values correspond to the proposed indices computed from curvature, first derivative, and second derivative features

Ice Condition	1	2	3	4	5	6
Curvature	0.985	0.998	0.929	0.492	0.782	*Graph*
First Derivative	0.787	0.615	0.789	0.504	0.826	*Graph*
Second Derivative	1.000	1.000	1.000	0.556	0.796	*Graph*

modified configurations were computed, and the contributions of the selected modes were summed, following the same procedure adopted in the numerical analysis.

During the campaign, ice was substituted with a paraffin layer, selected for its ease of use. While paraffin has a density comparable to ice, its Young's modulus is significantly lower, being between 40 and 100 times smaller. Accordingly, the tested configurations predominantly reproduce a mass effect rather than the stiffness increase that would result from ice. Six different paraffin patches were prepared, replicating the size and location of the numerical simulations with two exceptions: in Case 5 the patch exhibited a different irregular shape, and in Case 6 it was not possible to obtain a uniform thickness of 5 mm across the entire plate.

Figure 8 reports the experimental results obtained by applying the proposed localization algorithm to the six investigated configurations. Each row corresponds to a different paraffin patch, while the three columns display the outcomes obtained when using the curvature (first column), its first derivative (second column), and its second derivative (third column) as the input field for the algorithm.

A general trend can be observed across all cases. When curvature alone is employed, the localization is possible but relatively diffuse, and the estimated affected regions tend to spread over larger areas than the actual patch. The use of the first derivative of curvature does not improve the localization significantly; in fact, in most cases, the results are comparable to those obtained with curvature.

In contrast, the second derivative of curvature systematically provides clearer and more accurate results. The identified regions are more compact, better aligned with the actual paraffin patches, and less affected by spurious responses outside the damaged zones. This improvement is particularly evident in configurations 1, 2, and 3. In these cases, the second derivative highlights the modifications more sharply, reducing the influence of background variability.

The results reported in Table 3 confirm the numerical findings discussed in the previous section, showing that the second derivative of curvature constitutes the most effective indicator for experimental patch localization.

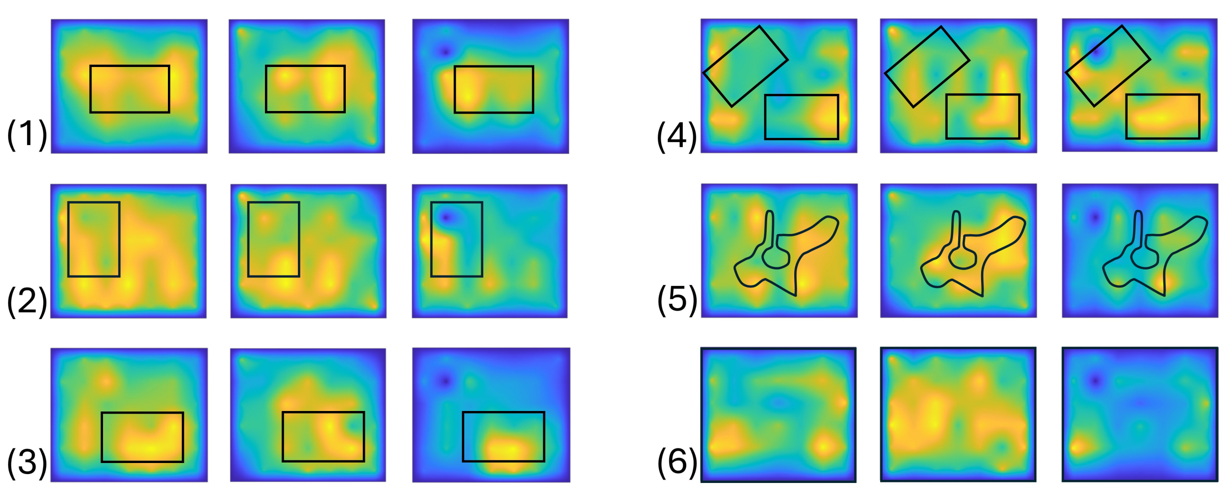

Fig. 8 Patch localization maps for the six analyzed configurations. Each row corresponds to a different scenario (Cases 1–6, see Table 1), while the three columns represent the localization algorithm applied to: (left) curvature mode shapes, (center) first spatial derivative of curvature mode shapes, and (right) second spatial derivative of curvature mode shapes. For each case, the approximate patch location is indicated in the figures. Warmer colors indicate stronger deviations from the reference, highlighting the regions most affected by paraffin accretion

Table 3 Experimental results of the localization performance index for the different conditions of paraffin. For Condition 6, where the patch covers the entire plate surface, the index is not informative and a qualitative graphical evaluation is reported instead

Ice Condition	1	2	3	4	5	6
Curvature	0.617	0.143	0.888	0.510	0.781	*Graph*
First Derivative	0.834	0.211	0.660	0.601	0.794	*Graph*
Second Derivative	0.889	0.789	0.911	0.884	0.713	*Graph*

Conclusion

This work presents a curvature-based approach, reconstructed through a network of piezoelectric sensors, for localizing ice on plate-like structures. Both numerical and experimental analyses have demonstrated that utilizing spatial derivatives of curvature enhances the method's sensitivity. In particular, the second derivative proved to be the most effective indicator, providing more compact, accurate, and robust reconstructions of the iced regions.

However, the use of the second derivative also introduces a significant drawback: it amplifies measurement noise. While this does not undermine the validity of the results obtained under controlled conditions, it limits the direct applicability of the algorithm in operational scenarios characterized by higher levels of disturbance. Therefore, the proposed method appears most suitable for applications where adequate noise control can be ensured, while further developments will be required to improve its robustness in real-world conditions.

Overall, the results confirm the potential of piezoelectric networks as a multifunctional platform for ice monitoring and autonomous management, paving the way for integrated sensing and de-icing solutions.

Acknowledgments This research was funded by the European Union – NextGeneration EU, Mission 4 Component 2 Investment 3.3 CUP B53C23001500004

References

1. Barber, S., Wang, Y., Jafari, S., Chokani, N., and Abhari, R.S. "The impact of ice formation on wind turbine performance and aerodynamics" (2011).
2. Lynch, F.T. and Khodadoust, A. "Effects of ice accretions on aircraft aerodynamics". *Progress in Aerospace Sciences*, 37(8):669–767 (2001).
3. Jarvinen, P. "Aircraft ice detection method". In *45th AIAA Aerospace Sciences Meeting and Exhibit*, page 696 (2007).
4. Wang, Y., Xu, Y., and Huang, Q. "Progress on ultrasonic guided waves de-icing techniques in improving aviation energy efficiency". *Renewable and Sustainable energy reviews*, 79:638–645 (2017).
5. Zhang, X., Zhou, W., and Li, H. "Electromechanical impedance-based ice detection of stay cables with temperature compensation". *Structural Control and Health Monitoring*, 26(9):e2384 (2019).
6. Maio, L., Memmolo, V., Christophel, N., Kohl, S., and Moll, J. "Electromechanical admittance method to monitor ice accretion on a composite plate". *Measurement*, 220:113290 (2023).
7. Wiedemann, J., Meyer, P., Feder, J., Sinapius, M., Riemenschneider, J., and Hühne, C. "Electromechanical deicing of helicopter structures with integrated ice detection by impedance measurement". *Journal of Aerospace Engineering*, 37(1):04023094 (2024).
8. Hongerholt, D.D., Willms, G., and Rose, J.L. "Summary of results from an ultrasonic in-flight wing ice detection system". In *AIP conference proceedings*, volume 615, pages 1023–1028. American Institute of Physics (2002).
9. Cuc, A., Giurgiutiu, V., Joshi, S., and Tidwell, Z. "Structural health monitoring with piezoelectric wafer active sensors for space applications". *AIAA journal*, 45(12):2838–2850 (2007).
10. Giurgiutiu, V., Bao, J., and Zhao, W. "Piezoelectric wafer active sensor embedded ultrasonics in beams and plates". *Experimental mechanics*, 43(4):428–449 (2003).
11. Giurgiutiu, V. "Tuned lamb wave excitation and detection with piezoelectric wafer active sensors for structural health monitoring". *Journal of intelligent material systems and structures*, 16(4):291–305 (2005).
12. Zhang, Y., Zhang, H., XIONG, J., et al. "Analysis method and experimental study of ice accumulation detection signal based on lamb waves". *Chinese Journal Of Aeronautics*, 37(8):388–403 (2024).
13. Pohl, M. "A lamb wave-based icing sensor for aircraft ice detection". In *Proceedings–Int. Workshop on Atmospheric Icing of Structures* (2022).
14. Zhao, X. and Rose, J.L. "Ultrasonic guided wave tomography for ice detection". *Ultrasonics*, 67:212–219 (2016).
15. Gantasala, S., Luneno, J.C., and Aidanpää, J.O. "Influence of icing on the modal behavior of wind turbine blades". *Energies*, 9(11):862 (2016).
16. Tsiapoki, S., Häckell, M.W., Grießmann, T., and Rolfes, R. "Damage and ice detection on wind turbine rotor blades using a three-tier modular structural health monitoring framework". *Structural Health Monitoring*, 17(5):1289–1312 (2018).

17. Pandey, A., Biswas, M., and Samman, M. “Damage detection from changes in curvature mode shapes”. *Journal of sound and vibration*, 145(2):321–332 (1991).
18. Wahab, M.A. and De Roeck, G. “Damage detection in bridges using modal curvatures: application to a real damage scenario”. *Journal of Sound and vibration*, 226(2):217–235 (1999).
19. Song, Z., Wei, J., and Li, F. “An accurate deicing method by utilizing the piezoelectric materials based on the active mode control theory”. *Mechanical Systems and Signal Processing*, 158:107804 (2021).
20. Whalen, T.M. “The behavior of higher order mode shape derivatives in damaged, beam-like structures”. *Journal of sound and vibration*, 309(3-5):426–464 (2008).
21. Robin, O., Chazot, J.D., Boulandet, R., Michau, M., Berry, A., and Atalla, N. “A plane and thin panel with representative simply supported boundary conditions for laboratory vibroacoustic tests”. *Acta Acustica united with Acustica*, 102(1):170–182 (2016).
22. Brandt, A. *Noise and vibration analysis: signal analysis and experimental procedures*. John Wiley & Sons (2023).